ADHESION OF DOPA FUNCTIONALIZED GELS TO SPIN LABELED SURFACES

A Thesis Submitted to
the Graduate School of Engineering and Sciences of
İzmir Institute of Technology
in Partial Fulfillment of the Requirements for the Degree of

MASTER OF SCIENCE

in Materials Science and Engineering

by
Yaman GÖKSEL

July 2017
İZMİR

We approve the thesis of **Yaman GÖKSEL**

Examining Committee Members:

Assoc. Prof. Dr. Yaşar AKDOĞAN
Department of Materials Science and Engineering, İzmir Institute of Technology

Asst. Prof. Dr. Ümit Hakan YILDIZ
Department of Chemistry, İzmir Institute of Technology

Asst. Prof. Dr. Osman AKIN
Department of Mechatronic Engineering, İzmir Katip Çelebi University

6 July 2017

Assoc. Prof. Dr. Yaşar AKDOĞAN
Supervisor, Department of Materials Science and Engineering,
İzmir Institute of Technology

Assoc. Prof. Dr. Mustafa EMRULLAHOĞLU
Co-Advisor, Department of Chemistry
İzmir Institute of Technology

Prof. Dr. Mustafa Muammer DEMİR
Head of the Department of Material Science and Engineering

Prof. Dr. Aysun SOFUOĞLU
Dean of the Graduate School of Engineering and Science

ACKNOWLEDGEMENTS

First of all, I am grateful for working with my supervisor, Assoc. Prof. Dr. Yaşar Akdoğan. Thanks to academic and personal guidance, his endless patience and support throughout this work. I would like to express my thanks to him cordially.

Also I would like to thank Asst. Prof. Dr. Ümit Hakan Yıldız and Asst. Prof. Dr. Osman Akın for participating as a committee member and reviewing my work.

I would like to thank my dear friends Anıl Özdemir, Begüm Demirkurt, Hakan Göktürk, İklima Kırpat and Tuğçe Semerci.

My special thanks to Assoc. Prof. Dr. Mustafa Emrullahoğlu for permission to enable using his laboratory facilities and his support on my thesis.

I would like to thank TÜBİTAK (114Z318) and IZTECH for supporting me during this project.

Endless gratitude is also extended to my family, Sibel Vural, Göksel Göksel, Alp Soloğlu and Nebile Bab for their endless support and their firm faith that I can achieve whatever I set my mind on. Finally, I would like to thank my S.O. Şeyma İşlek deep from my hearth for being my morally and motivationally compass throughout years.

ABSTRACT

ADHESION OF DOPA FUNCTIONALIZED GELS TO SPIN LABELED SURFACES

This study investigates the force free adhesive properties of synthetic polymer in aqueous media using electron paramagnetic resonance (EPR) spectroscopy.

Due to poor performance of commercial adhesives in wet environments, scientists are interested in different types of adhesives to overcome this difficulty. On this context, mussels attract attention because of their versatile properties to adhere different types of surfaces from rocks to ship hulls underwater. Adhesion occurs when mussel secretes mussel foot proteins (MFPs) in order to form threads and plaques. Seven types of MFPs are unique in plaque contains high amount of L-3,4-dihydroxyphenylalanine (DOPA) amino acid which is reputed to be responsible for adhesion.

In this research, branched polyethylene glycol (PEG) based polymers functionalized with DOPA were synthesized and their force-free adhesive properties to hydrophobic polystyrene and hydrophilic silica nanobeads were investigated in solution. These nanobead surfaces were conjugated with spin label molecules to probe adhesion dynamics using EPR spectroscopy. In addition, gel forms of polymers obtained using $NaIO_4$, $FeCl_3$ and Cr_2O_7 were used as adhesive materials for EPR measurements. All of these adhesive materials showed adhesion to spin labeled polystyrene (SL-PS) surface. However, non-DOPA containing PEG showed no indication of adhesion thus, demonstrating the importance of DOPA in wet adhesion. In addition, EPR results showed that DOPA based PEG polymers were unable to adhere to spin labeled silica (SL-SiO_2) surface. This behavior was attributed to hydration layers around silica nanobeads. These layers formed around hydrophilic SiO_2 surface prevent interaction between nanobead surface and polymeric material.

ÖZET

DOPA FONKSİYONELLEŞTİRİLMİŞ JELLERİN SPİN ETİKETLİ YÜZEYLERE YAPIŞMASI

Bu çalışmada sualtı organik yapışkan malzemelerin sentetik polimer benzerlerinin kuvvet uygulamadan, ıslak ortam yapışma özellikleri araştırılmıştır.

Islak ortamda zayıf yapışkanlık özellikleri gösteren ticari yapıştırıcılar, bilim insanlarının ilgisini bu sıkıntıları giderecek farklı tiplerde yapıştırıcılar üzerine çekmiştir. Bu bağlamda midyeler gemi gövdesinden kayalara kadar farklı tip yüzeylere ıslak ortamda yapışabilme özellikleri sayesinde oldukça ilgi çekicidir. Yapışma proteinli midye plaklarının midye ayağı proteinlerini (MFP) salgılaması sonucu oluşan iplikçiklerin yüzeylere tutunması sonucu gerçekleşir. Sadece midye plaklarına özgü 7 tip MFP yapısında yüksek miktarda bulunan L-3,4-dihidroksifenilalanin (DOPA) amino asiti yapışmadan sorumlu olarak görülmektedir.

Bu araştırmada 4 kollu polietilen glikol (PEG) bazlı polimer mimikleri ve hidrofobik polistiren ve hidrofilik silica nanokürelerin yüzeyine onların kuvvet uygulamadan yapışma özellikleri solusyon içinde incelenmiştir. Bu nanoküreler, yüzeylerindeki yapışma dinamiklerinin EPR spektroskopisi ile incelenmesi için spin etiketli moleküller ile konjuge edilmiştir. Ayrıca, DOPA fonksiyonel polimerlerin $NaIO_4$, $FeCl_3$ and Cr_2O_7 ile elde edilmiş hidrojel formları dahil olmak üzere tüm yapışkan malzemeler spin etiketli polistiren nanokürelerin yüzeyinde iyi yapışma performansı sergilemiştir. DOPA taşımayan polimerlerin yapışkanlık özelliği sergilememesi DOPA'nın sualtı yapışkanlığı için önemini göstermektedir. Buna ek olarak, DOPA fonksiyonel polimerlerin spin etiketli silika nanokürelerin ($SL\text{-}SiO_2$) yüzeyine yapışmadığını gösterilmiştir. Hidrofilik yüzey etrafında oluşan hidrasyon tabakası silika nanoküre yüzeyi ile polimerik malzemelerin temasını engellemektedir.

To my family

TABLE OF CONTENTS

LIST OF FIGURES

Figure **Page**

LIST OF TABLES

LIST OF ABBREVIATIONS

DOPA	L-3,4-dihydroxyphenylalanine
MFPs	Mussel Foot Proteins
SL-PS	Spin Labeled Polystyrene Nanobeads
SL-SiO_2	Spin Labeled Silica Nanobeads
BSA	Bovine Serum Albumin
DCM	Dichloromethane
DMF	N,N-dimethlyformamide
DMSO	Dimethyl Sulfoxide
MES	2-(*N*-morpholino)ethanesulfonic acid
PEG	Polyethylene glycol
NaCl	Sodium Chloride
NaHCO	Sodium Bi-carbonate
Na_2SO_4	Sodium Sulfate
$FeCl_3$	Iron(III) chloride hexahydrate
Cr_2O_7	bis(tetrabutylammonium) dichromate
$NaIO_4$	sodium (meta) periodate
HOBT	1-hydroxybenzotriazol
EPR	Electron Paramagnetic Resonance
NMR	Nuclear Magnetic Resonance
UV-Vis	Ultraviolet-visible
SFA	Surface Force Apparatus
Boc	di-tert-butyl-dicarbonate
DMF	N,N-dimethlyformamide
HBTU	2-(1H-benzotriazol-1-yl)-1,1,3,3-tetramethyluronium hexafluorophosphate

CHAPTER 1

INTRODUCTION

1.1. Mussel Foot Proteins (MFPs)

Biomimicry is one of the most useful way for mankind to solve complex problems. This is widely used in almost every engineering discipline. As the name suggests, this field of science has focused on imitating living creatures. Inspired from shark scales ability to reduce turbulence of swimming, Speedo created a new type of bodysuit for swimmers which was used by most of the Olympic athletes participated in 2008 Summer Olympics where a total of 25 new world records were set. N. nucifera (lotus) plant has super hydrophobic and self-cleaning properties caused by nanostructures on surface epidermal cells covered with wax tubules. This structure was imitated to make self-cleaning coat fabrics and also was used as anti-fog surface coatings. From the working mechanism of surface hairs on climbing bean plant P. vulgaris and cockleburs, a commercial zipper-like product was developed called Velcro which we use at many textile products like gloves, jackets, shoes etc. Engineers replicated humpback whales' flippers low drag creating architecture in commonly used wind turbine blades. One can find other examples of how nature overcomes difficulties that we are looking for the solutions (Bhushan, 2009).

Marine organisms are also inspirational creatures in this context. Man-made adhesives have poor performance when they were introduced to wet surfaces (Adams, 1983). Yet barnacles and mussels stick on different types of surfaces underwater. Their adhesions endure harsh marine environment as their versatile nature helps them to cling on metal, rock or even organic surfaces. These features of mussels draw attention of many research groups, and understanding their adhesion mechanism opened up many possible applications from surgical tissue adhesive (Cencer *et al*., 2014) to magnetic resonance imaging (Na *et al*., 2012).

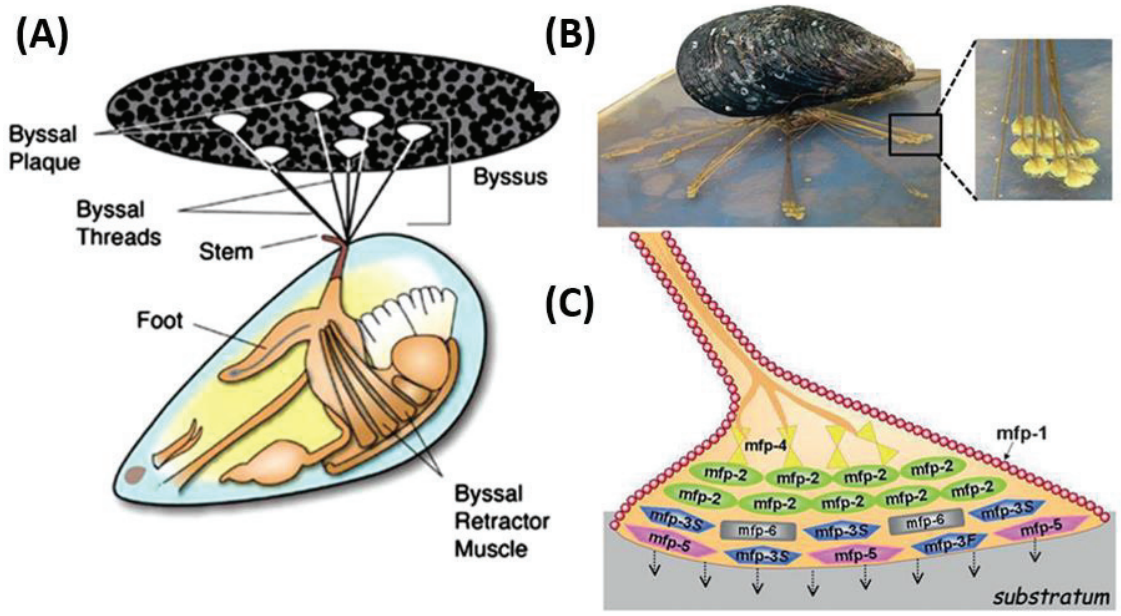

Figure 1.1. (A) Schematic structure of blue mussel (M. edulis) (Source: Silverman, 2007). (B) A mussel (Mytilus californianus) attached to surface. (C) Distributions of different Mussel foot proteins (MFPs) in a plaque of Mytilus californianus (Source: Akdogan *et al*., 2014).

Mussel anatomy have been investigated by many research groups. Figure 1.1. shows anatomy of a blue mussel. Most mussel species use plaques to adhere to external surfaces. To achieve adhesion, the mussel foot extends to the surface and secrete proteinacious plaques. After creating these plaques, mussel foot disconnects itself from plaques and retreats to the mussel shell while leaving protein threads that connect plaques to shell. 10 to 40 threads connect an average mussel to its plaques in order to withstand harsh marine environment (Waite, 1992).

There are roughly 25 - 30 different types of mussel foot proteins (MFPs). Only 7-8 of them are unique for the plaque. Table 1 shows MFPs found in plaque and some of their properties. As seen in Figure 1.1. (C), proteins that are found at outer surface of plaque (MFP-1, MFP-3 and MFP-5) have high L-3,4-dihydroxyphenylalanine (DOPA) amino acid content. These MFPs were further investigated for their adhesion properties by many scientists (Lee at al., 2011).

Table 1.1. Proteins of synthesized by Mytilus byssus (Source: Lee *et al*., 2011).

Protein	Mass (KDa)	pI	DOPA mol%	Location of protein
Mefp-1	~110	10	10–15	Cuticle
Mefp-2	~40/45	9	3–5	Plaque
Mefp-3	~5–7	8–10	20–25	Plaque
Mefp-4	~70–80	10.5	5	Plaque
Mefp-5	~9.5	9–10	30	Plaque
Mefp-6	~11.6	10	4	Plaque
PreCol-D	~80	9	<1	Thread/ plaque
PreCol-P	~95	9	<1	Thread/ plaque
PreCol-NG	~76	9	<1	Thread/ plaque

For mussels to stick on surface there are two important works have to be done by these proteins in plaques and threads. They have to adhesively hold on surface and also have to cohesively hold each other and keep the structural integrity of the threads. Crosslinking between proteins plays an important role in the cohesive interactions.

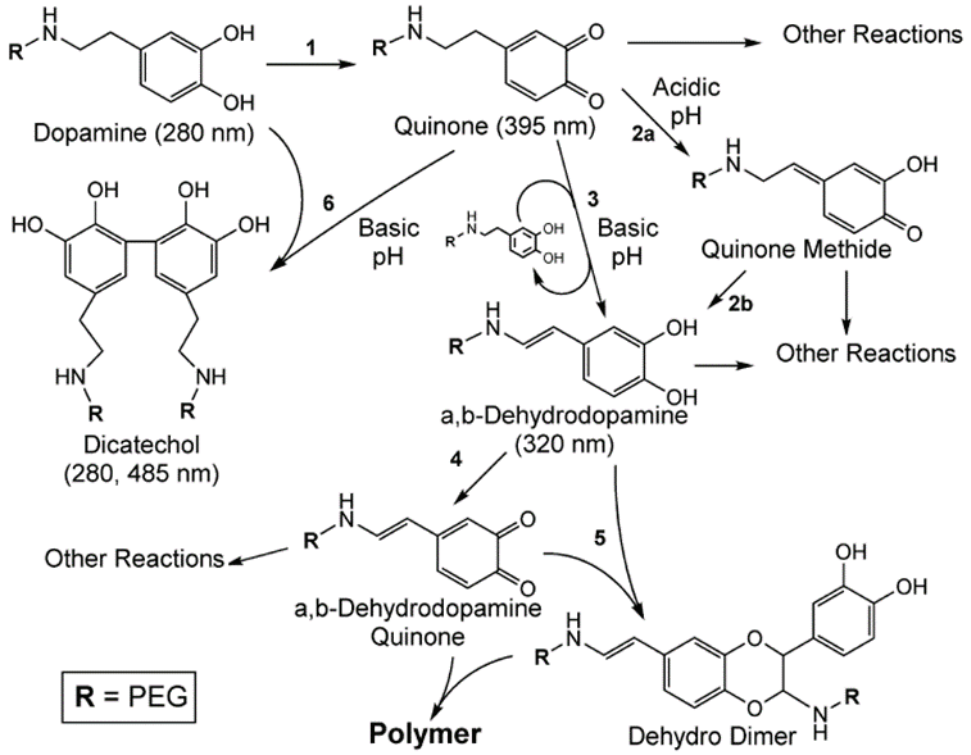

Figure 1.2. Possible pathways of DOPA oxidation in a polymerization reaction (Source: Cencer *et al*., 2014).

Catechol moiety of DOPA amino acid plays an important role in the adhesion. It has hydroxyl groups that can form hydrogen bonding with appropriate hydrophilic surfaces. Catechol groups can be easily oxidized either with an oxidizer or at basic pH, and they reversibly turn into highly reactive quinone (which has carbonyl groups instead of hydroxyl) that causes covalent crosslinking. At acidic pH quinone turns into quinone methide which is reactive with organic compounds. Quinone methide can later turn into α,β-dehydrodopamine. At basic pH values, quinone can skip this step and directly turns into α,β-dehydrodopamine. This intermediate can further turn into other reactions' intermediates like α,β-dehydrodopamine quinone or a dehydro dimer which can cause crosslinking. Basic pH values can also cause dicatechol formation from either catechol or quinone (figure 1. 2.) (Cencer *et al*., 2014).

On the other hand, DOPA can form coordination bonds with many multivalent metal ions (Xu, 2013). Fe, Mn, Zn, Ca, Ti ions form mono, bis and tris coordinations with DOPA. Since there are no covalent bonds in these coordination complexes, this kind of crosslinking is reversible after breaking, which explains self-healing behavior observed

in mussel adhesion. Example of these coordination compounds formed with iron ions can be seen at figure 1.3.

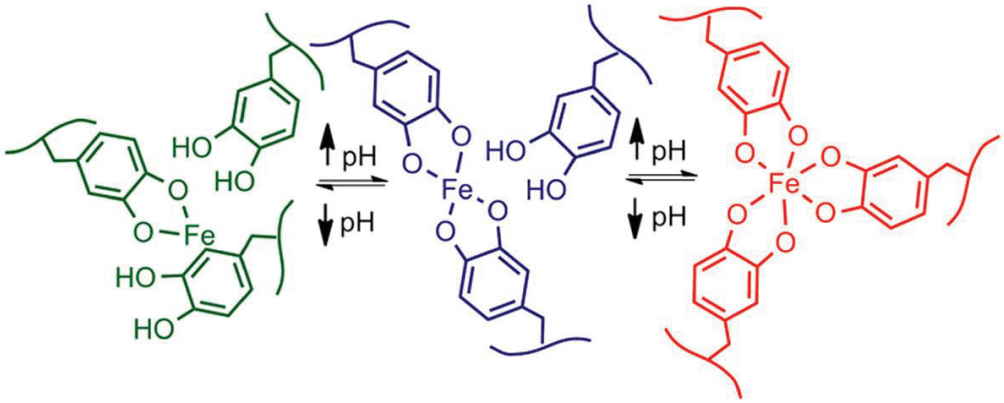

Figure 1.3. Formation of mono, bis and tris coordination at different pH values with Fe, respectively from left (Source: Krogsgaard *et al*., 2013).

Surface force apparatus (SFA) is mainly used to understand how MFPs adhere to various surfaces. Danner *et al*. (2012) showed that MFP-5 adhesion on mica surface is directly affected by DOPA oxidation. Increasing pH of the medium or addition of $NaIO_4$ caused oxidation of hydroxyl groups on DOPA and diminished adhesion to mica. On the other hand, oxidized DOPA groups (either with pH increase or with an oxidizer) provide strong cohesion with crosslinking between MFPs.

Adhesion of MFPS to TiO_2 surfaces showed the same kind of behavior (Anderson *et al*., 2010). At pH 3, strong adhesion was observed but addition of $NaIO_4$ or raising pH to 5.5 suppressed sticking on surface. Even further increasing pH to 7.5 showed an increase in surface adhesion. Increasing pH has two contradicting effects. First is oxidizing of DOPA and losing its ability to form H-bonding with oxygen containing surfaces. Second is increasing ability of forming DOPA-Ti coordination bonds. At higher pH values second effect became more effective and the formed bonds are appeared to be stronger than H-bonding (Yu *et al*., 2013 b). SFA experiments showed that MFPs can also attach to hydrophobic surfaces. It is not possible to form hydrogen bonding in such case. Leucine, isoleucine, phenylalanine and most importantly tryptophan are hydrophobic groups can be found in different MFPs that can cause hydrophobic

interaction with hydrophobic surfaces. DOPA can also interact with hydrophobic surfaces with its aromatic ring (Yu *et al*., 2013 a).

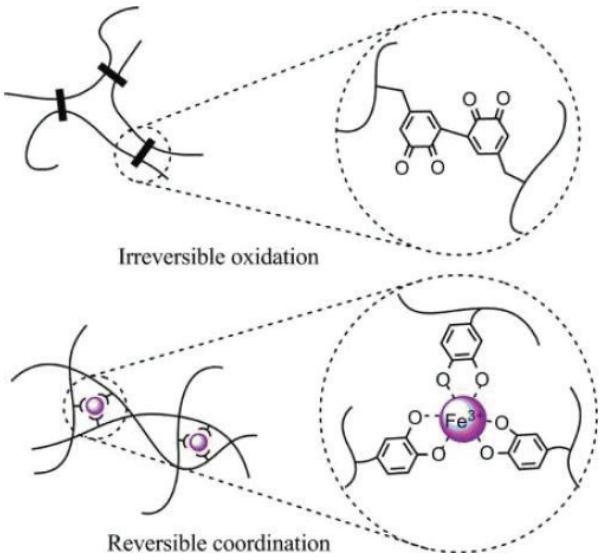

Figure 1.4. Comparison of reversible coordination and irreversible covalent bonding crosslinking (Source: Xu *et al*., 2012)

Forming coordination bonds with metals, hydrogen bonding with hydrophilic surfaces and making hydrophobic interactions with many different hydrophobic surfaces make adhesion reversible, versatile and also remarkably strong. On the other hand, making covalent bonds with organic surfaces causes irreversible bond formation but ability to form covalent bonds with organic molecules makes mussel adhesion can be used also in biological applications (figure 1.4).

1.2. DOPA Functionalized Polymers

MFPs are not possible candidate for a mass produced adhesive due to their delicate extraction methods and handling conditions. On the other hand, synthesizing DOPA functionalized polymers inspired by MFPs are cost-effective and easy to fabricate and handle. Conjugating a polymer end group with DOPA is the main approach in synthesizing these materials. There are different types of polymers backbones like polyethylene glycol (PEG) (Eberle *et al*., 2000), polymethyl methacrylate (Güvendirek *et*

al., 2008), polysiloxane (Heo *et al*., 2012) etc., with different polymer conformations. The most abundant material in the literature is 4-arm PEG end functionalized with DOPA that is protected with di-tert-butyl dicarbonate (Boc) group (Figure 1.5).

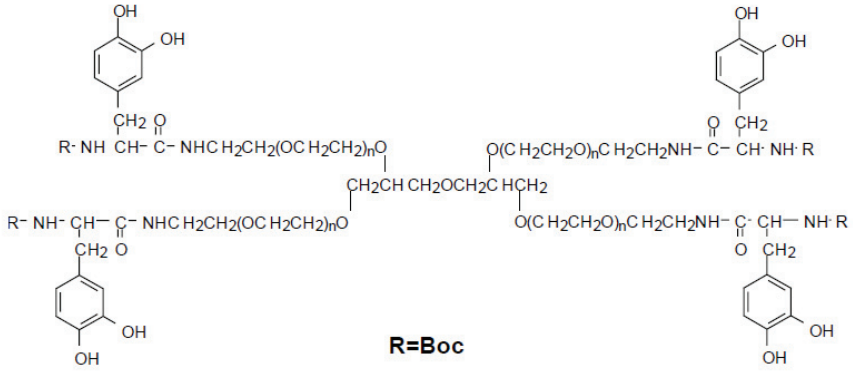

Figure 1.5. Structure of PEG-(N-Boc-DOPA)$_4$
(Source: Eberle *et al*., 2000).

UV-Visible (UV-Vis) spectroscopy has been used to investigate the mechanism of hydrogel formation of DOPA conjugated polymers. Quinone signal appeared around 395 nm immediately upon addition of $NaIO_4$ (Figure 1.6). As time passed this signal decreased while α,β-dehydrodopamine signal at 325 nm increased. Other reaction intermediates and pathways can be seen in figure 1.2.

In another case, each coordination complexes formed with iron ions at different pH values show different UV-Vis spectra. At pH 5 mono complexes were formed with absorptions at 450 nm and 650 nm, at pH 7 bis complexes occurred with a strong absorption, around 570 nm. Furthermore, increasing pH up to 12 makes tris complexes dominant and absorption blue shifted down to 500 nm. On the other hand, below pH 5 coordination complexes became unstable. Around pH 3 covalent bonds between DOPA molecules were formed in the presence of Fe^{3+} ions (figure 1.7) (Xu *et al*., 2012).

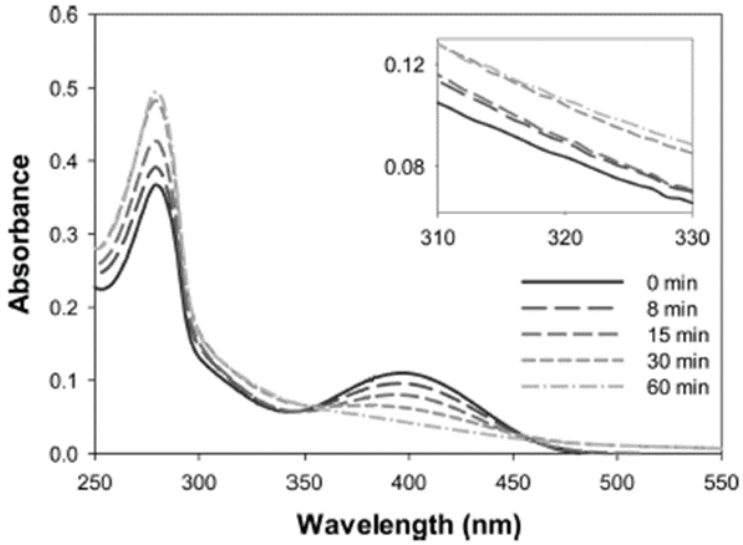

Figure 1.6. UV Visible spectra of PEG-(N-Boc-DOPA)$_4$ solution containing $NaIO_4$ (Source: Cencer *et al*., 2014).

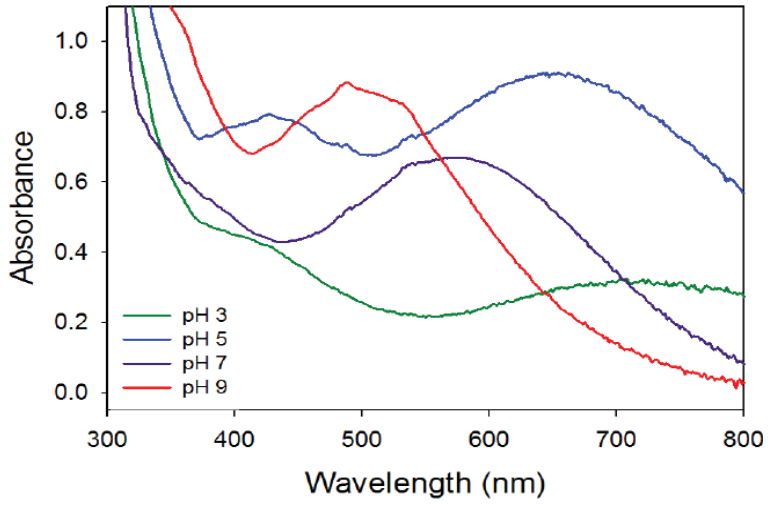

Figure 1.7. UV Visible spectrum of PEG-(N-Boc-DOPA)$_4$ solution containing Fe^{3+} (Source: Barrett *et al*., 2012).

Self-healing properties of PEG-(N-Boc-DOPA)$_4$ hydrogels are much like coordination cross-linked MFPs. Fe^{3+} induced hydrogels take prior shape after a while (figure 1.8.). Due to the unrepairable broken covalent bonds $NaIO_4$ hydrogels could not get their prior when cut in half.

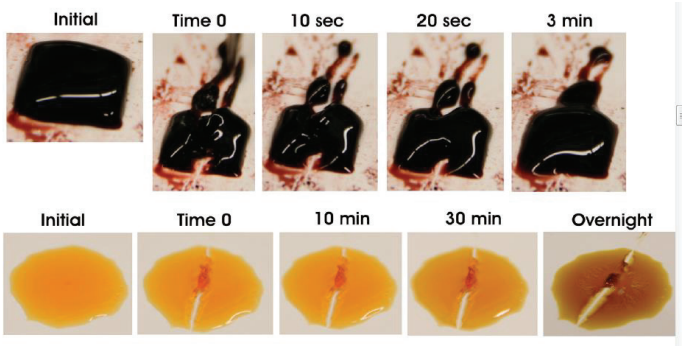

Figure 1.8. Self-healing coordination hydrogel made with using Fe^{3+} (top), non-self-healing covalent bonded hydrogel made with $NaIO_4$ (bottom) (Source: Holten-Andersen *et al*., 2011).

1.3. Electron Paramagnetic Resonance (EPR) Spectroscopy

Pauli Exclusion Principle states that maximum two electrons with opposite spin properties occupy an orbital at a time. These two opposite spins "cancel out" each other in terms of spin magnetism. Semi-occupied orbital electrons cause a spin magnetic moment which can be analyzed with Electron Paramagnetic Resonance (EPR) spectroscopy. EPR technique measures resonant absorption of electromagnetic radiation by an unpaired electron. Free electron spin magnetic moment is given by:

$$\mu_{ez} = -g_e \beta_e S_z$$

where g_e is free electron (correction) Zeeman factor also known as g factor. β_e is Bohr magneton and $\hat{S}_z$ is electron spin operator. Interactions between external applied magnetic field B with this spin magnetic moment μ is defined by energy U.

$$U = -\mu^T . \mathrm{B} = -B^T . \mu = -|\mu \mathrm{B}| \cos(\mu, \mathrm{B})$$

Term (μ,B) defines angle between B and μ. When magnetic field is applied, unpaired electron can only have at one of two energy states (M_s =+1/2 or -1/2). Higher energy state occurs when the direction of spin magnetic moment is opposite to the direction of magnetic field, and lower energy state occurs when they are both aligned.

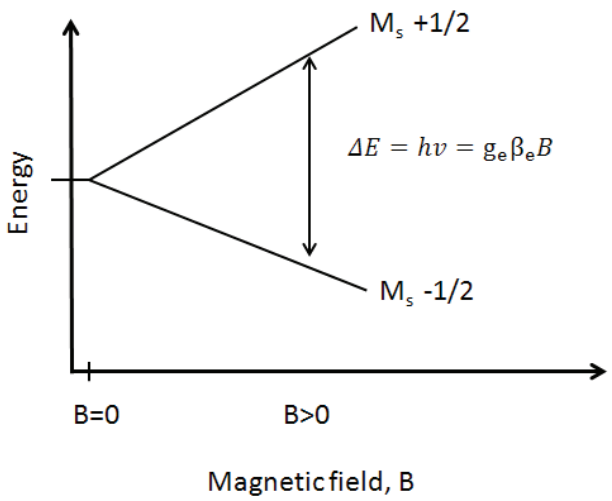

Figure 1.9. Energy diagram of a system that has an unpaired electron in an external magnetic field.

These energy levels are called Zeeman energy levels and the interaction between B and μ is called Zeeman interaction. When energy difference (ΔE) between energy levels of spin states that separated by applied magnetic field equals to the energy of the microwave frequency (hv), unpaired electron changes its spin state by absorbing this microwave radiation. In other words, at resonance conditions external magnetic field excites the unpaired electron from lower state to upper state.

$$\Delta E = h\nu = g_e\beta_e B$$

Additionally, magnetic moment created by electron orbital motion contributes to total magnetic moment applied to the free electron. This moment perturbs pure spin ground state and it causes spin-orbit interaction.

There are three g values depending on axis system of molecule called g_x, g_y and g_z. When paramagnetic ion system has an isotropic shape, these g values equal to each other. In cases where distortions cause an anisotropy in paramagnetic ion system, anisotropic spectra obtained where $g_x \neq g_y \neq g_z$.

Disturbances on rotational motion of electron further effect the EPR absorption spectrum with an anisotropic fashion. Many hindering effects on rotational motion cause these changes on spectra which can also give important information of system.

Another coupling interaction is caused by nuclear spin (I≠0) which is called hyperfine interactions. This interaction splits energy, and the number of splits calculated by the 2nI+1 (where n is the number of the effective nucleus and I is the nuclear spin number) equation (Akdogan, 2009).

EPR absorbance measurements are generally analyzed after taking the first derivative of the spectra. This is widely used procedure because taking first derivative helps to observe minor differences in the absorbance spectra.

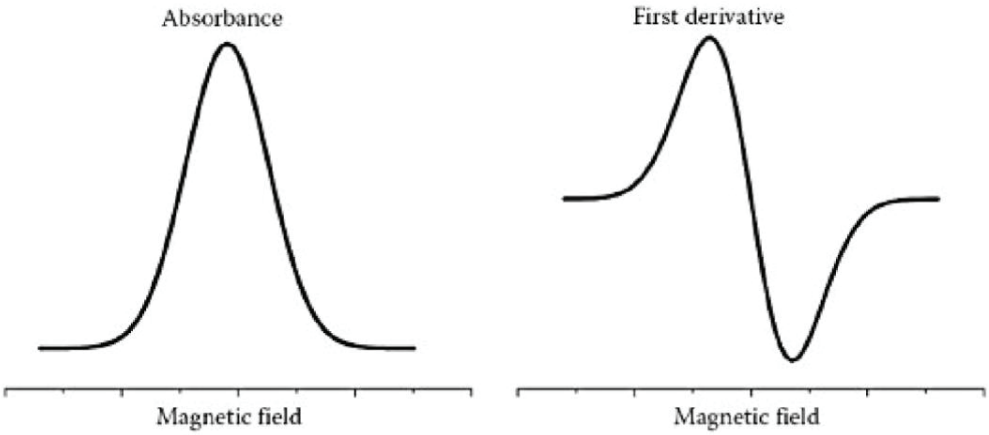

Figure 1.10. Common absorbance spectra (left) and its first derivative (right) (Source: Talsi and Bryliakov, 2017).

As discussed above EPR can only analyze paramagnetic materials. This setback can be overcome by attaching a spin label molecule on a diamagnetic material which makes the sample EPR active (Akdogan *et al*. 2016; Tatlidil *et al*. 2015). One of the most commonly used spin label molecule is 2,2,6,6-Tetramethylpiperidin-1-yl) oxyl (TEMPO). For example, 4-carboxy-Tempo (figure 1.11) attaches to surface through the functional groups on surface.

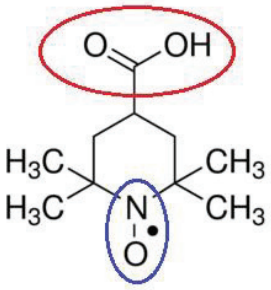

Tempo-4-carboxylate

Figure 1.11. Functional group (red circle) and radical group (blue circle) of 4-carboxy-Tempo.

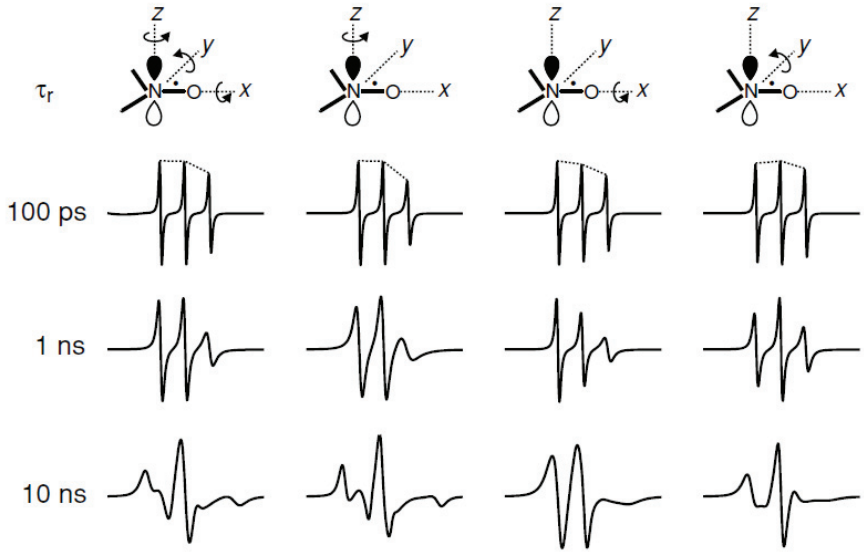

Figure 1.12 ESR spectra of stable nitroxide radical when it has fast and slow motions with regards to spin axis in aqueous medium (Source: Hinderberger and Jeschke, 2008).

For TEMPO, EPR signal splits into 3 lines because of ^{14}N nucleus (n=1 and I=1) and has a g value around 2.0. Figure 1.12 shows the changes in nitroxide radical EPR spectrum depending on the rotational correlation motion. Since rotational motion speed is directly affected by its surrounding environment it can probe even a slight distortion. Akdogan *et al*. used this feature to investigate adhesion of MFPs. Spin labeled polystyrene (SL-PS) and spin labeled silica (SL-SiO_2) nanobeads mixed with MFPs in

solution were studied using the variation of EPR signal shape (Fig. 1. 12) (Akdogan *et al*. 2014).

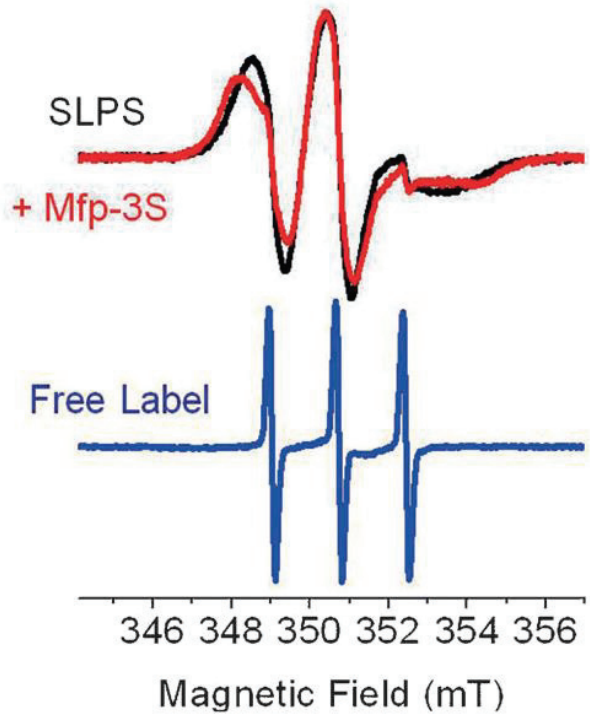

Figure 1.13. EPR signal change after adhesion of MFP-3 on polystyrene surface (Source: Akdogan *et al*., 2014).

Rotational speed of spin label molecules slows down drastically after their binding on polystyrene surface. Additionally, adhesion of MFP-3 proteins to polystyrene surface further hindered bound spin label rotational motion. Rotational correlation time of free spin labels was found as 20 ps and it slowed down to 4.2 ns when attached to polystyrene surface. Furthermore, adhesion of MFP-3 to SL-PS slowed down the rotational correlation time of spin label to 5.7 ns (Akdogan *et al*., 2014).

CHAPTER 2

EXPERIMENTAL STUDY

2.1. Materials

Materials used in this work are amine modified polystyrene nanobeads (50 nm diameter, Sigma Aldrich), 3-aminopropyl functionalized Silica (d<100nm Sigma Aldrich), 4-carboxy-Tempo (Sigma Aldrich), N-(3-dimethylaminopropyl)-N'-ethylcarbodiimide hydrochloride (EDC, 99%, Sigma Aldrich), ultra-centrifugal tubes (50 kDa cut-off, Merck), 3,4 dihydroxy-L-phenylalanine (98%, Sigma), di-tert-butyl-dicarbonate (99%, Aldrich), 2-(1H-benzotriazol-1-yl)-1,1,3,3-tetramethyluronium hexafluorophosphate (HBTU, 98%, Acros Organics), 1-hydroxybenzotriazol (HOBT, 97% Aldrich), ethyl acetate (99,5%, Sigma Aldrich), 1-4-dioxane (99,8% extra dry, Arcos Organics), 4arm-PEG-NH_2 (10kDa, Laysan Bio. Inc.), triethylamine (99%, Acros Organics), N,N-dimethlyformamide (DMF, 99,7%, ABCR), dichloromethane (DCM, 99,9 VWR Chemicals), hydrochloric acid (HCl, 37% Sigma Aldrich), sodium sulfate (Na_2SO_4, 99%, Sigma Aldrich), sodium chloride (NaCl, 99,8%, Sigma Aldrich), sodium bicarbonate ($NaHCO_3$, 99,7%, Sigma Aldrich), bovine serum albumin (BSA, 96% lyophilized powder, Sigma), Iron(III) chloride hexahydrate (97%, Sigma Aldrich), 2-(N-morpholino)ethanesulfonic acid (MES) buffer anhydrous (high purity, Amresco), bis(tetrabutylammonium) dichromate (99%, Sigma Aldrich), sodium (meta) periodate (99,5%, Sigma), used without further purification.

EPR was measured with Adani CMS 8400 electron paramagnetic resonance spectrometer (Adani, Belarus). UV-Vis spectra were obtained with UV-2550 UV-Visible spectrometer (Schimadzu, Japan). EPR spectra were normalized and simulated using Easyspin 4.5.5 Matlab software package. (Stoll and Schweiger, 2006)

2.2. Synthesis of PEG-(N-Boc-DOPA)$_4$

2.2.1. Synthesis of N-Boc-DOPA

Triethylamine (86 µL) and L-DOPA (78.85 mg, 0.4 mmol) were mixed in DCM:Dioxane (1:1) solution (800 µL) at 0 ºC (ice bath). Later, di-tert-butyl dicarbonate (98 mg, 0.45 mmol) dissolved in dioxane (400 µL) was added into the first mixture and was stirred for 30 min. The solution was mixed at room temperature for 17 hours. Afterwards, solution was extracted with 50 mL ethyl acetate, and pH of the organic phase adjusted to 1 by adding HCl. Later this solution was back extracted with ethyl acetate 3 more times. Organic phase was dried with Na_2SO_4, and was evaporated to obtain N-Boc-DOPA as brown gel (Giorgioni *et al*., 2010). ^{1}H NMR (400 MHz, DMSO-d_6) δ: 6.87 (d, 1H), 6.58 (d, 2H), 6.44 (d, 1H), 4.01-3.93 (m, 1H), 2.79-2.58 (m, 2H), 1.30 (s, 9H).

2.2.2. Synthesis of PEG-(N-Boc-DOPA)$_4$

PEG-(NH_2)$_4$ (97 mg, 9.7x10-3 mmol), N-Boc-DOPA (23.9 mg, 80 mmol), HOBT (17.3 mg, 0.128 mmol), and triethyl amine (17.6 µL) were mixed in 920 µL of DCM:DMF (1:1) solution at 25 ºC. Later HBTU (29.6 mg, 0.078 mmol) in 460 µL DCM was added into solution and mixed for 5 hours. The solution was washed with saturated NaCl solution, $NaHCO_3$ (5% w/ml) solution, HCl (1 M) solution (50 ml), and distilled water (50 ml), respectively. Final organic phase was dried with Na_2SO_4 and precipitated in cold diethyl ether for 3 times to afford PEG-(N-Boc-DOPA)$_4$ (Lee *et al*., 2002). ^{1}H NMR (400 MHz, $CDCl_3$) δ: 6.76 (t, 8H), 6.57 (d, 4H), 6.14 (s, 4H), 4.20 (s, 4H), 3.79 (t, 8H), 3.62-3.39 (m, 896H), 3.02 (d, 8H), 2.72 (t, 8H), 1.41 (s, 36H).

2.2.3. Synthesis of Spin Labeled Polystyrene (SL-PS) and Spin Labeled Silica (SL-SiO_2) Nanobeads

Amine modified polystyrene beads (100 µL) was added in 4-carboxy-Tempo solution (250 µL, 10 mM) in MES buffer (0.2 M) at pH 3. Solution was gently mixed while drop wise addition of EDC (90 µL, 38 mM) and left for overnight at room

temperature (RT). The mixture was washed with MES buffer using centrifuge concentrator tubes 10 times (70 000 rpm, RT, 5 min for each cycle). Then solution was concentrated down to 20 μL for further measurements.

Amine modified silica beads (100 μL) was added in 4-carboxy-Tempo solution (250 μL, 10 mM) in MES buffer (0.2 M) at pH 3. Solution was gently mixed and EDC (90 μL, 38 mM) was added drop wise. Afterwards, reaction was left for overnight at RT. Mixture was washed using centrifuge concentrator tubes 10 times with MES buffer at 70 000 rpm. The solution was concentrated down to 100 μL for further experiments (Akdogan *et al*., 2014).

2.2.4. PEG-(N-Boc-DOPA)$_4$ Hydrogel Preparation

PEG-(N-Boc-DOPA)$_4$ stock solution was prepared in MES buffer (0.2 M pH 3) with polymer concentration at 360 mg/mL (32.4 mM) where DOPA concentration of this solution is 129,6 mM. Cross-linkers used in this work as follows; iron (III) chloride hexahydrate ($FeCl_3$), sodium (meta) periodate ($NaIO_4$), bis(tetrabutylammonium) dichromate (Cr_2O_7). Cross-linker solutions were prepared at concentrations corresponding to DOPA amount (8.1 mM) with desired DOPA:cross-linker ratios as DOPA:Fe^{+3}, DOPA:IO_4^- DOPA:$Cr_2O_7^{2-}$, and were mixed at 1/1 v/v ratio with PEG-(N-Boc-DOPA)$_4$ solution where polymer concentration was 45 mg/mL. After mixing, immediately solution colors were changed to green, orange, purple for $FeCl_3$, $NaIO_4$, Cr_2O_7 cross-linkers respectively (Holten-Andersen *et al*., 2010). All hydrogels were cured until gel form obtained before mixing with spin labeled nanobead solutions. All desired adhesive materials added into spin labeled nanobead solutions with 1/1 v/v ratio for EPR measurements.

CHAPTER 3

RESULTS AND DISCUSSION

3.1 Characterization of Hydrogel Formation with UV-Vis Spectroscopy

UV-Vis spectroscopy was used to investigate the formation of cross-linked PEG-(N-Boc-DOPA)$_4$ hydrogels. First of all, we used UV-vis spectroscopy to show the PEG-DOPA conjugation in MES buffer at pH 3.0 (figure 3.1). The absorption signal at 290 nm corresponds to the catechol group in DOPA. PEG-$(NH_2)_4$ does not have an absorption signal. Furthermore, a new absorption signal appears at 395 nm upon addition of $NaIO_4$ as an oxidizing agent.

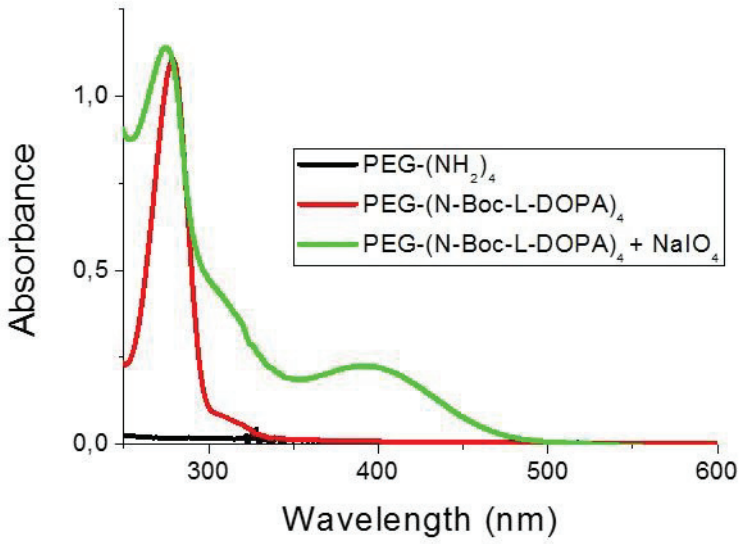

Figure 3.1. UV-vis spectra of PEG-$(NH_2)_4$ (black), PEG-(N-Boc-DOPA)$_4$ (red), and PEG-(N-Boc-DOPA)$_4$ + $NaIO_4$ conjugation (green) (Source: Kırpat *et al*., 2017).

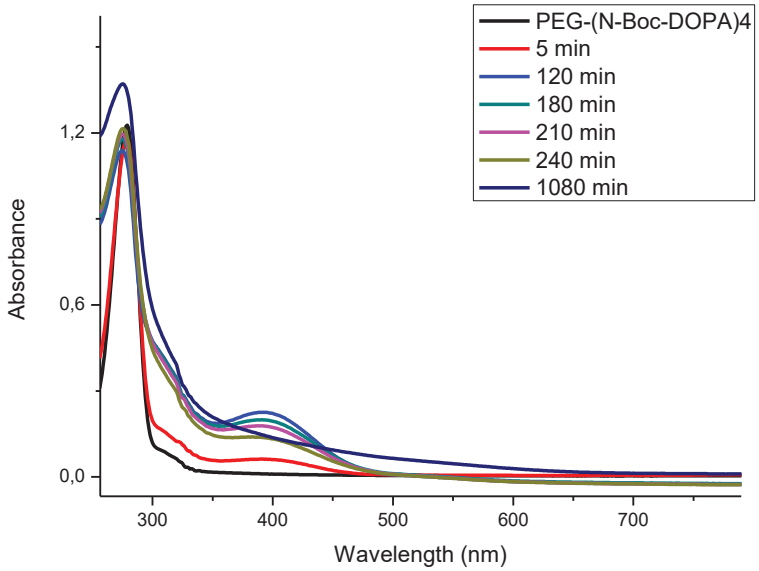

Figure 3.2. UV-Vis spectra of PEG-(N-Boc-DOPA)$_4$ (123 μM) before and after addition of $NaIO_4$ (1488 μM) with time (in MES buffer at pH=3.0).

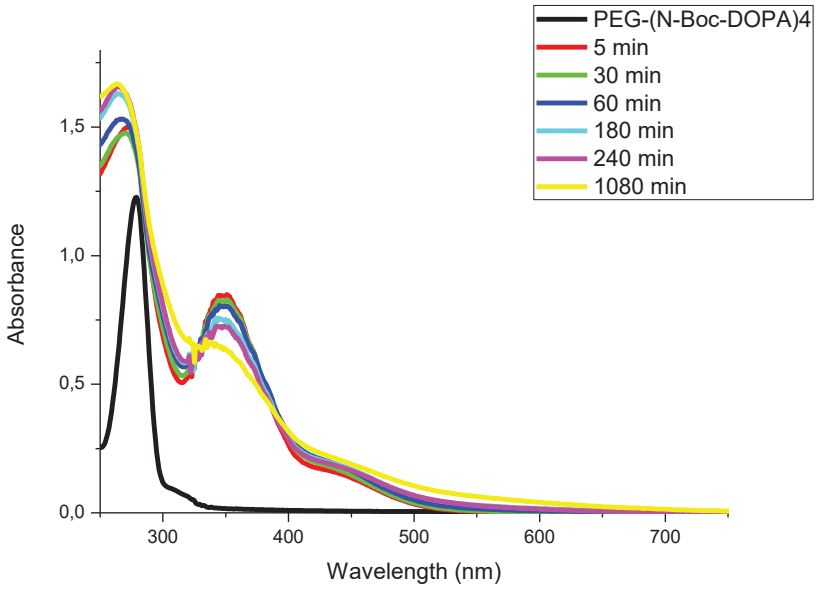

Figure 3.3. UV-Vis spectra of PEG-(N-Boc-DOPA)$_4$ (123 μM) before and after addition of Cr_2O_7 (496 μM) with time (in MES buffer at pH=3.0).

UV-Vis spectra of hydrogels formed with different cross-linkers are different. Addition of $NaIO_4$ immediately oxidized catechol groups into quinone. Quinone signal first increased and after 2 hours the signal started to decrease. Quinone intermediates turned into α, β-dehydrodopamine with time which caused the increase in absorption around 325 nm. Interpretation of catechol absorption at 290 nm is unfeasible since as gelation proceeds other byproducts that appear around the same wavelength makes spectra obscure (figure 3.2). This behavior has been also seen in many literature works for covalent bonded gel crosslinking (Cencer *et al*., 2014). Also, in the case of Cr_2O_7 containing hydrogels, longer gelation time decreases the absorption peak of quinone (figure 3.3).

On the other hand, addition of $FeCl_3$ gives different UV-Vis spectra than spectra obtained from hydrogel formed with other oxidizers. Quinone signal and also mono, bis and tris signals were not observed. At pH 3 these coordination complexes are not favorable compared to covalent bonded crosslinking therefore quinone signal was not observed.

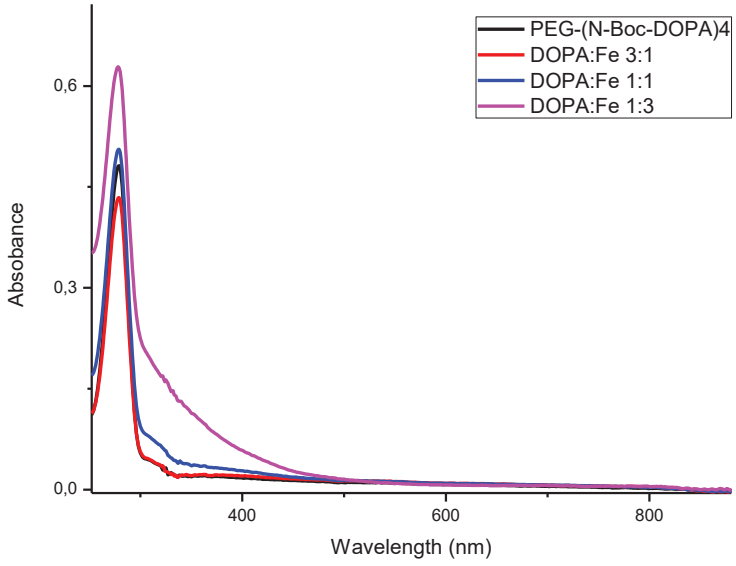

Figure 3.4. UV-Vis spectra of PEG-(N-Boc-DOPA)$_4$ (123 µM) before and after 2 hours addition of $FeCl_3$ with 3 different DOPA:Fe ratios; 3:1 (164 µM), 1:1 (492 µM) and 1:3 (1488 µM) (in MES buffer at pH=3.0).

Figure 3.4 shows the UV-Vis spectra of PEG-(N-Boc-DOPA)$_4$ upon addition of $FeCl_3$ with different DOPA:Fe ratios (3:1, 1:1 and 1:3) after 2 hours. After $FeCl_3$ addition,

only a broadening around 330 nm was observed in all spectra, except the sample with a ratio of 3:1 (Barrett *et al*., 2012; Holten-Andersen *et al*., 2011).

3.2. Adhesion of PEG-(N-Boc-DOPA)$_4$ and Hydrogels to SL-PS and SL-SiO_2 Surfaces

4-carboxy-Tempo and its conjugation with nanobeads were studied with EPR spectroscopy (Fig. 3.4). EPR line shape of 4-carboxy-Tempo gives important information about rotational dynamics of spin label molecule.

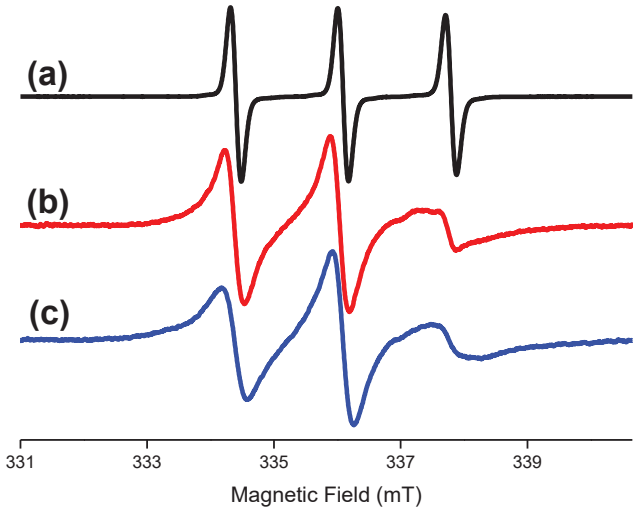

Figure 3.5. EPR spectra of a) free 4-carboxy-Tempo b) SL-PS and c) SL-SiO_2 (in MES buffer at pH=3.0).

Figure 3.5 shows the EPR spectra of free 4-carboxy-Tempo, SL-PS and SL-SiO_2 in MES buffer at pH 3.0. EPR signal shape of the 4-carboxy-Tempo drastically changed when it binds to the surface of PS or SiO_2. By simulation of EPR spectrum of free 4-carboxy-Tempo, the rotational correlation time was found as τ_R = 20 ps. However, the rotational correlation time increased up to 2.8 ns and 2.9 ns after attached to the surface of PS and SiO_2, respectively. After conjugation reaction, excess spin label molecules were washed away with centrifuge process. EPR signals of SL-PS and SL-SiO_2 have no indication of free 4-carboxy-Tempo signal, thus it was concluded that there were no free

spin label molecules left in solutions.

Addition of PEG-(N-Boc-DOPA)$_4$ to SL-PS solution changed the shape of the SL-PS EPR spectrum. Figure 3.6 shows how EPR signal of SL-PS changes when PEG-(N-Boc-DOPA)$_4$ adhere to SL-PS surface. Dashed arrows show the formation of second type of signal. As concentration of PEG-(N-Boc-DOPA)$_4$ increases in solution, this new signal appears to be more intense.

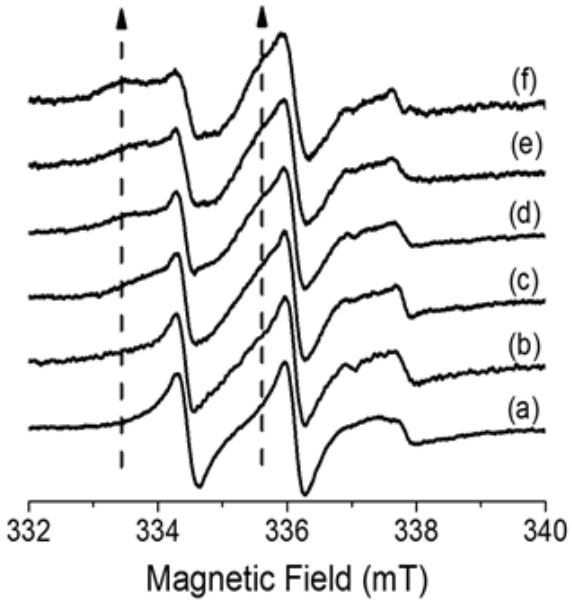

Figure 3.6. EPR spectra of SL-PS before a) and after addition of PEG-(N-Boc-DOPA)$_4$ with final concentrations of b) 11 mg/mL, c) 22 mg/mL, d) 45 mg/mL, e) 90 mg/mL, f) 180 mg/mL (in MES buffer at pH=3.0) (Source: Kırpat *et al*., 2017).

Addition of PEG-(N-Boc-DOPA)$_4$ increased τ_R value up to 10 ns which shows the further hindering rotational movement of the radical center. This is the direct indication of PEG-(N-Boc-DOPA)$_4$ coverage over spin label molecules on PS surface. Percentage of covered and uncovered spin labels on PS surface can be found with the simulation of the EPR spectra. The area under each EPR spectrum is related with the number of spin labels bound to PS. Addition of appropriate ratios of simulated covered and uncovered spin label signals gives experimental EPR spectrum. The percentages of covered and uncovered spin labels on PS were found 68% and 32%, respectively in the case of 45 mg/mL PEG-(N-Boc-DOPA)$_4$, (Fig. 3.6). Other simulations with different PEG-(N-Boc-

DOPA)$_4$ concentrations and their surface coverage ratios are shown in figure 3.8 and figure 3.9, respectively.

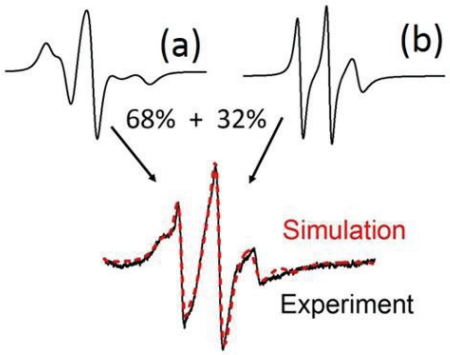

Figure 3.7. Simulations of EPR spectra of a) covered and b) uncovered spin labels on PS with appropriate proportions produce the experimental result of 45 mg/mL PEG-(N-Boc-DOPA)$_4$ (Source: Kırpat *et al*., 2017).

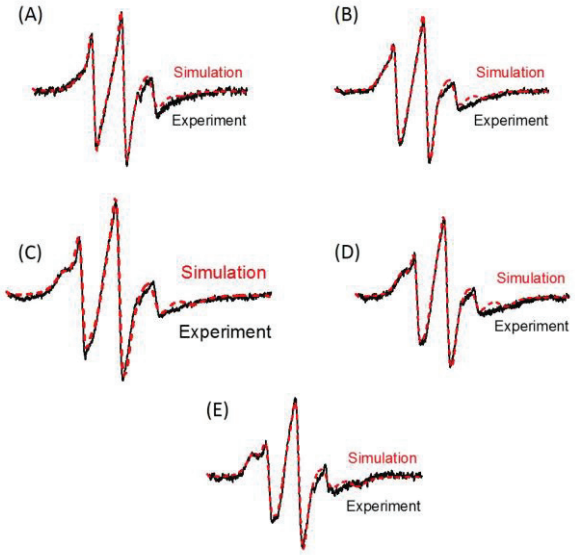

Figure 3.8. EPR spectra of SL-PS and their simulations after addition of PEG-(N-Boc-DOPA)$_4$ at final concentrations of a) 11 mg/mL, b) 22 mg/mL, c) 45 mg/mL, d) 90 mg/mL, and e) 180 mg/mL (in MES buffer at pH 3.0) (Source: Kırpat *et al*., 2017).

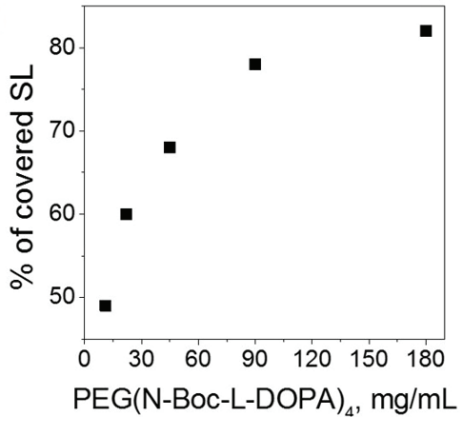

Figure 3.9. Percentage of covered spin label molecules on PS upon addition of the PEG-(N-Boc-DOPA)$_4$ with varying concentrations (Source: Kırpat *et al*., 2017).

Furthermore, PEG-$(NH_2)_4$ was used to investigate whether any binding can be attributed to polymer backbone or not. EPR spectra of SL-PS before and after polymer addition were same which proved that the adhesion was caused by the presence of DOPA molecules (figure 3.10).

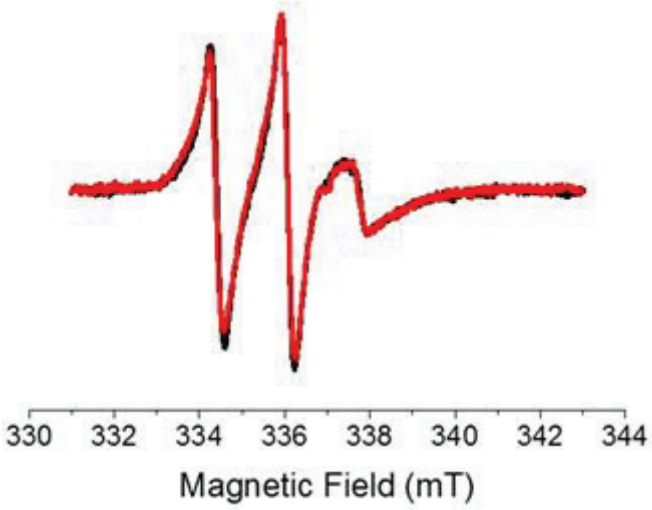

Figure 3.10. EPR spectra of SL-PS (black) and after addition of PEG-$(NH_2)_4$ (in MES buffer at pH 3.0) at final concentration of 90 mg/mL (red) (Source: Kırpat *et al*., 2017).

Adhesion of hydrogel form of PEG-(N-Boc-DOPA)$_4$ to SL-PS was measured by EPR spectroscopy. Figure 3.11 shows EPR spectra of SL-PS after addition of hydrogels

obtained with $FeCl_3$, $NaIO_4$ and Cr_2O_7 on SL-PS surface. For all hydrogels PEG-(N-Boc-DOPA)$_4$ concentration was set to 45 mg/mL.

$FeCl_3$ including hydrogels are better than $NaIO_4$, and Cr_2O_7 hydrogels showed more adhesion compared to other hydrogels.

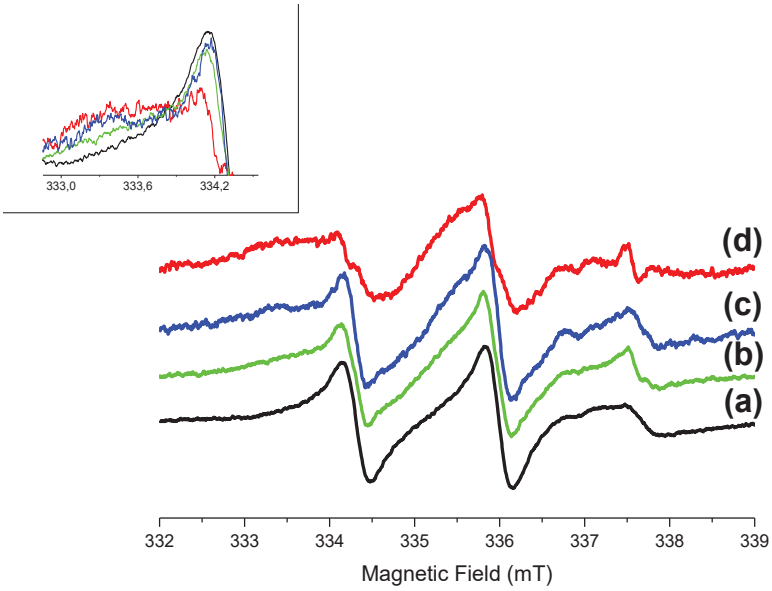

Figure 3.11. EPR spectra SL-PS a) before and after addition of hydrogels prepared with b) $NaIO_4$, c) $FeCl_3$, d) Cr_2O_7 (final concentration of PEG-(N-Boc-DOPA)$_4$ is 45 mg/mL in MES buffer at pH=3.0, DOPA:cross-linker ratio of hydrogels is 1:1).

As literature suggests, Cr_2O_7 formed hydrogels are more stiff and perform better at lap shear tests (Westwood *et al.*, 2007). In contrary, it was expected that $NaIO_4$ performed better than $FeCl_3$ hydrogels. This finding may be caused due to difference of pH values used in literature and in here. The pH values are 3 and 7 in our experiments and in the literature, respectively.

Figure 3.12 shows the EPR spectra of SL-SiO_2 before and after addition of PEG-(N-Boc-DOPA)$_4$. The EPR line shape did not change upon addition of PEG-(N-Boc-DOPA)$_4$. This shows that PEG-(N-Boc-DOPA)$_4$ did not adhere to SiO_2 surface significantly.

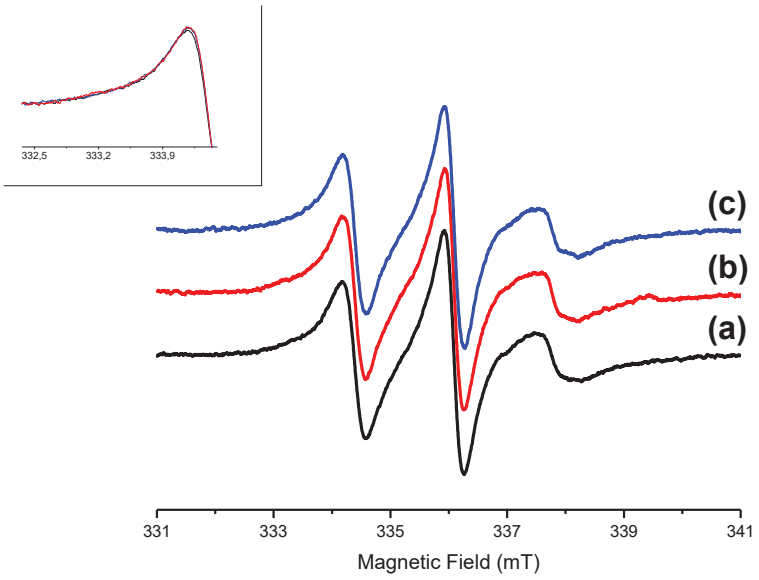

Figure 3.12. EPR spectra of SL-SiO_2 a) before and after addition of PEG-(N-Boc-DOPA)$_4$ with final concentrations of b) 45mg/mL, c) 90mg/mL (in MES buffer at pH=3.0, inset shows left-hand signal of overlaid spectra).

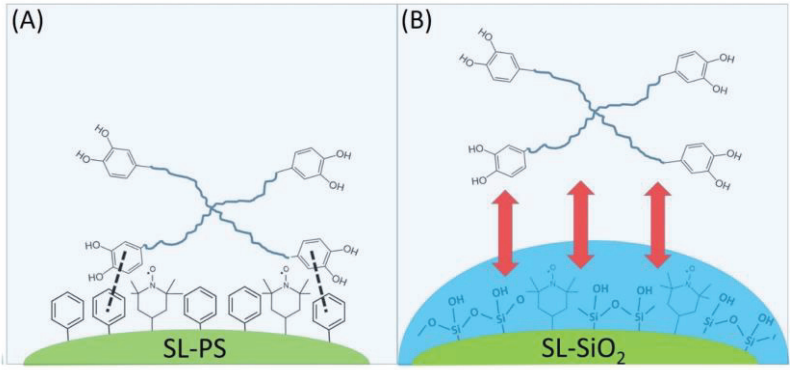

Figure 3.13. Schematic representations of PEG-(N-Boc-DOPA)$_4$ adhesion on a) SL-PS and b) SL-SiO_2 (Source: Kırpat *et al*., 2017).

Hydrophilic SiO_2 nanobeads have strong hydration layers around themselves. These strong hydration layers prevent PEG-(N-Boc-DOPA)$_4$ adhesion by repelling molecules away from surface. Compared to SiO_2 surface, hydrophobic PS have weak hydration layers. Therefore, PEG-(N-Boc-DOPA)$_4$ can adhere to PS surface. Schematic representation of this phenomena was shown in figure 3.13.

Hydrogel form of PEG-(N-Boc-DOPA)$_4$ obtained with $NaIO_4$ with a 45 mg/mL polymer concentration is, also acted like non-hydrogel form and showed no significant

adhesion to silica surface. As shown in Figure 3.14, EPR spectra of SL-SiO_2 and hydrogel added SL-SiO_2 with different cross-linker ratios overlap with no indication of adhesion.

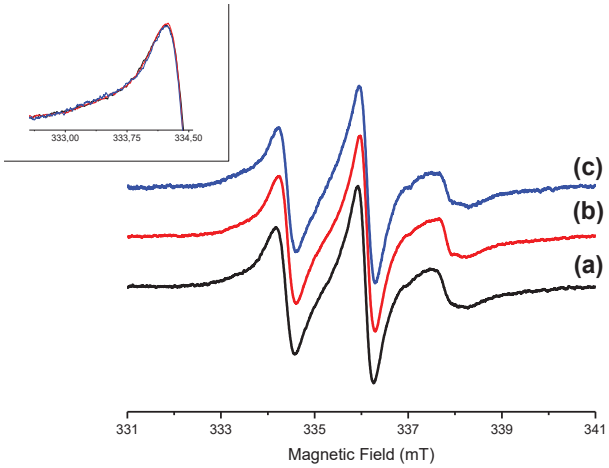

Figure 3.14. EPR spectra of a) bare SL-SiO_2 and after addition of $NaIO_4$ hydrogel (45 mg/mL PEG-(N-Boc-DOPA)$_4$ concentration) with DOPA:cross-linker ratios of b) 1:1, c) 1:3 (in MES buffer at pH=3.0, inset shows left-hand signal of overlaid spectra).

Interestingly, $FeCl_3$ hydrogel with 1:3 DOPA:cross-linker ratio shows indication of adhesion in contrary to $NaIO_4$ hydrogel. Slight difference between hydrogel and SL-SiO_2 can be seen in Figure 3.15 inset.

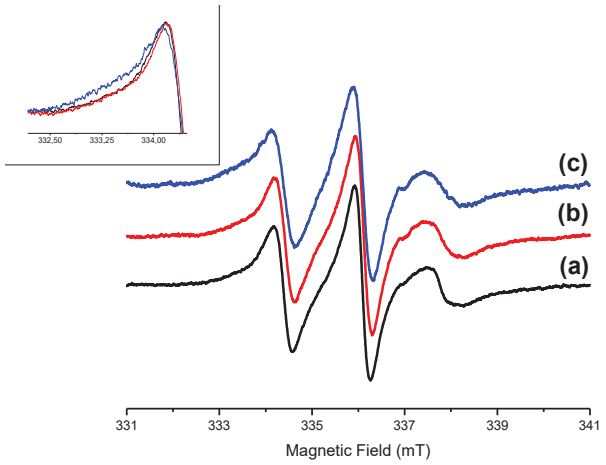

Figure 3.15. EPR spectra of a) bare SL-SiO_2 and after addition of $FeCl_3$ hydrogel (45 mg/mL PEG-(N-Boc-DOPA)$_4$ concentration) with DOPA:cross-linker ratios of b) 1:1, c) 1:3 (in MES buffer at pH=3.0, inset shows left-hand signal of overlaid spectra).

As expected from its adhesion on SL-PS surface, Cr_2O_7 included hydrogels are also able to break hydration layers and cover spin label molecules on SiO_2 surface. Figure 3.16 shows the adhesion of Cr_2O_7 hydrogel adhesion on SL-SiO_2. Inset of the figure shows the indication of adhesion of hydrophilic surface. This suggests that hydrogels with high cross-linker content can break these hydration layers.

Schematic representation of hydration layers' effect to adhesion on nanobead surface and to EPR signal of spin label molecules are shown in figure 3.17.

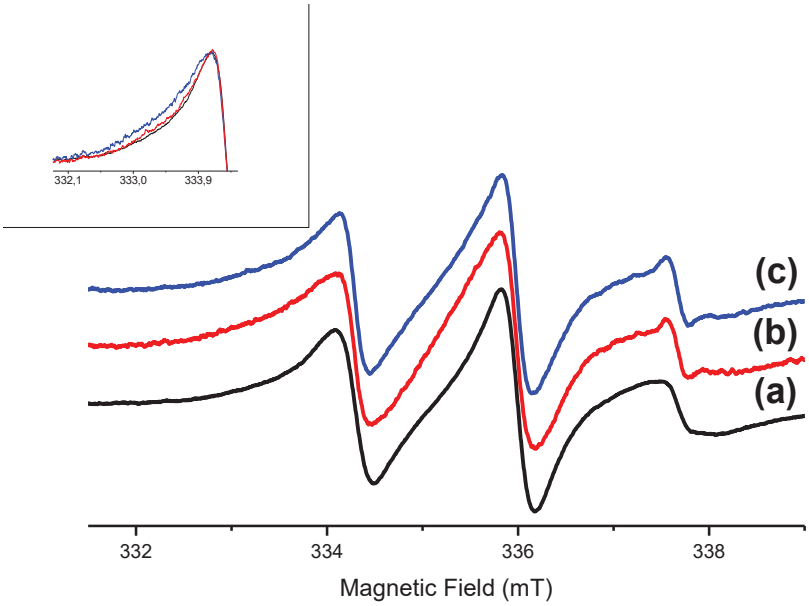

Figure 3.16. EPR spectra of a) bare SL-SiO_2 and after addition of Cr_2O_7 hydrogel (45 mg/mL PEG-(N-Boc-DOPA)$_4$ concentration) with DOPA:cross-linker ratios of b) 1:1, c) 1:3 (in MES buffer at pH=3.0, inset shows left-hand signal of overlaid spectra).

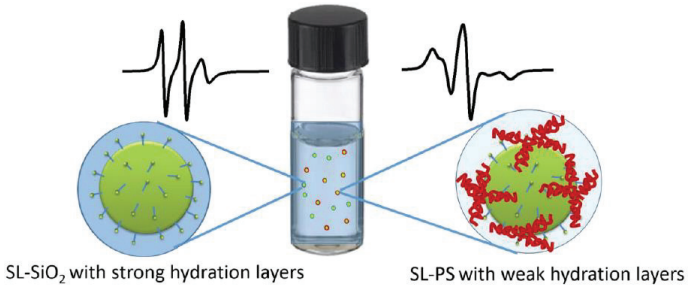

Figure 3.17. Schematic representation of PEG-(N-Boc-DOPA)$_4$ adhesion on hydrophilic and hydrophobic surfaces (Source: Kırpat *et al*., 2017).

3.3. Adhesion of BSA to SL-PS and SL-SiO$_2$ surfaces

Adhesion of BSA was also tested on SL-PS surface. BSA has been readily used in many different biological applications for its versatile adhesion properties (Su and Pelton, 2006). The used highest final sample concentration was limited to 90 mg/mL because of the solubility limit of BSA.

Increasing BSA concentration in SL-PS mixture significantly affected adhesion to nanobead surface. Figure 3.18 shows increasing adhesion with increasing BSA concentration. Similar to PEG-(N-Boc-DOPA)$_4$, increasing BSA concentration positively effects nanobead surface coverage.

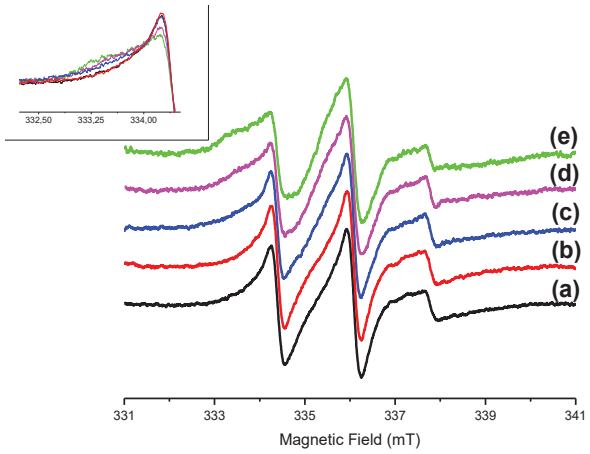

Figure 3.18. EPR spectra of SL-PS before a) and after addition of BSA with final concentrations of b) 4.5 mg/mL, c) 22.5 mg/mL, d) 45 mg/mL and e) 90 mg/mL (in MES buffer at pH=3.0, inset shows left-hand signal of overlaid spectra).

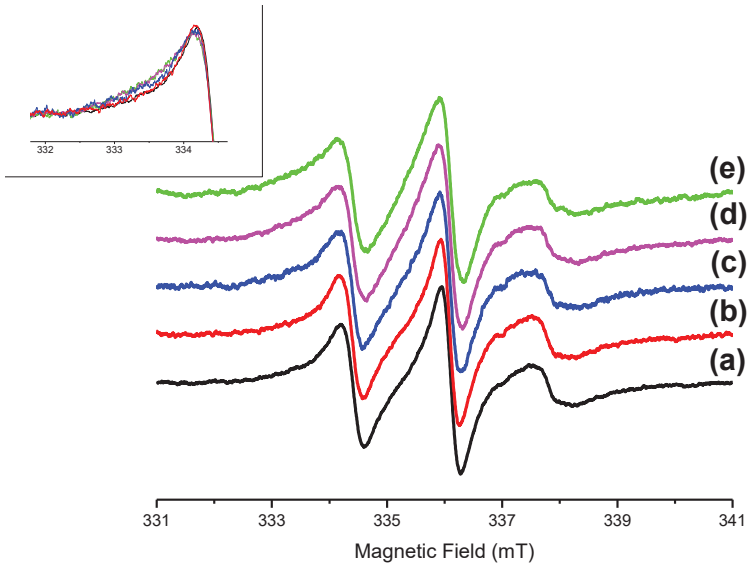

Figure 3.19. EPR spectra of SL-SiO_2 a) before and after addition of BSA with final concentrations of b) 4.5 mg/mL, c) 22.5 mg/mL, d) 45 mg/mL, e) 90 mg/mL (in MES buffer at pH=3.0, inset shows left-hand signal of overlaid spectra).

On the other hand, BSA molecules can weakly adhere to SL-SiO_2 especially when 90 mg/mL BSA is used (Figure 3.19). This is due to hydrophobic amino acid groups contained in BSA structure are able to break through these hydration layers and make adhesion possible.

3.4. EPR Spectra of 4-carboxy-Tempo with Adhesive Materials and Cross-linkers

Finally, effects of these adhesive materials on the EPR spectrum of free 4-carboxy-Tempo were examined. Figure 3.20 shows that only $FeCl_3$ hydrogel makes a difference in the spectrum of free spin label molecule. This effect is due to spin exchange reaction between 4-carboxy-Tempo and Fe ions (Hussain *et al*., 2009). This reaction causes the EPR signal broadening.

The same spin exchange effect was seen in EPR spectra when only the cross-linker material, $FeCl_3$, was added into 4-carboxy-Tempo solution. However, addition of $NaIO_4$ and Cr_2O_7 did not cause a spin exchange reaction and broadening, as shown in Figure 3.21.

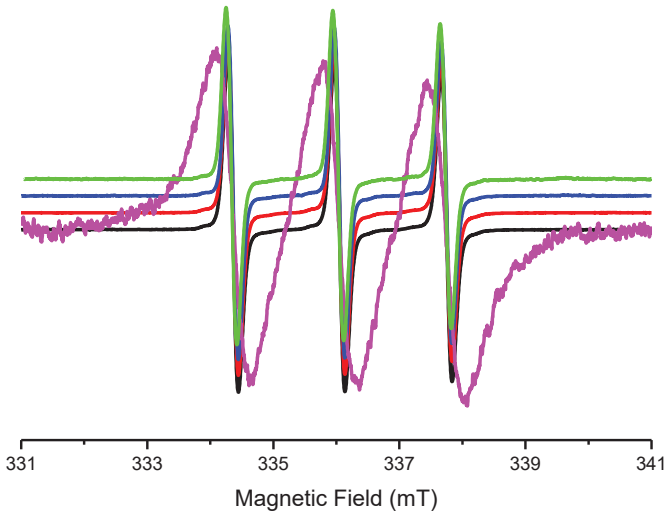

Figure 3.20. EPR spectra of 4-carboxy-Tempo (1 mM) and after addition of PEG-(N-Boc-DOPA)$_4$ (45 mg/mL), $NaIO_4$, $FeCl_3$ and Cr_2O_7 included hydrogels (polymer concentration 45 mg/mL) with DOPA:cross-linker ratios were 1:3 shown in black, red, blue, magenta and green lines, respectively (in MES buffer at pH=3.0).

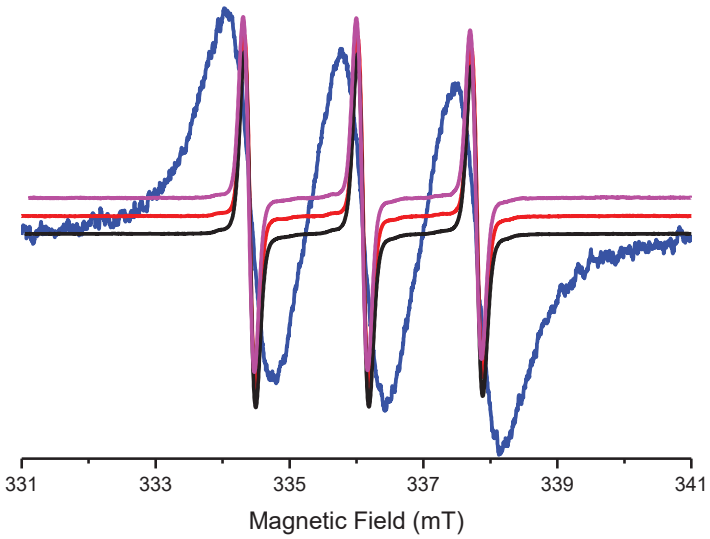

Figure 3.21. EPR spectra of 4-carboxy-Tempo before and after addition of $NaIO_4$ (192 mM), $FeCl_3$ (192 mM) and Cr_2O_7 (192 mM) cross-linkers shown in black, red, blue and magenta lines, respectively (in MES buffer at pH=3.0).

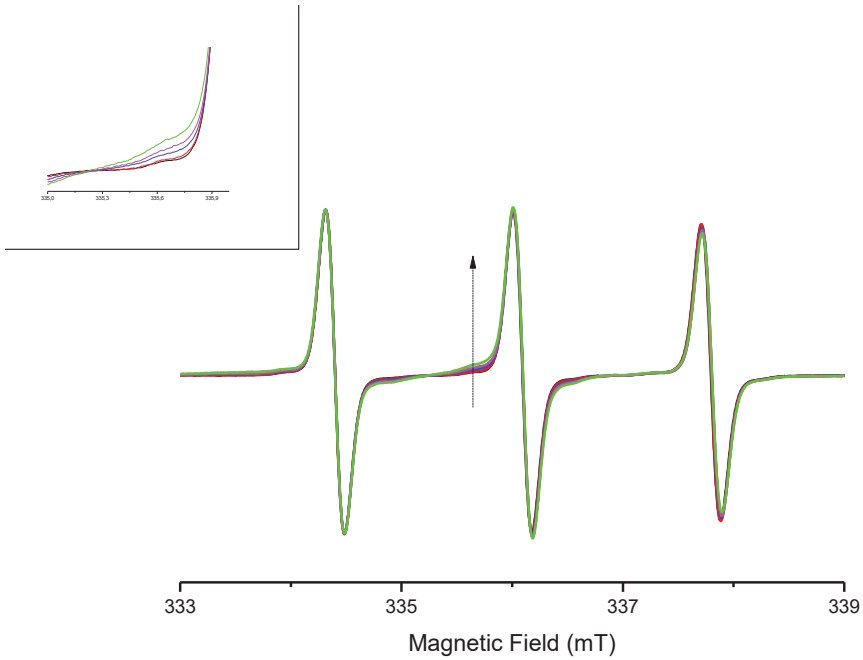

Figure 3.22. EPR spectra of 4-carboxy-Tempo and after addition of BSA with final concentrations of 4.5 mg/mL, 22.5 mg/mL, 45 mg/mL, 90 mg/mL shown in black, red, blue, magenta and green lines respectively (in MES buffer at pH=3.0, inset shows middle signal of overlaid spectra).

BSA solution with different concentrations were mixed with free spin label molecule (1 mM) solution (Figure 3.22). Free spin label molecules bind to BSA molecule. BSA has 583 amino acid residues that some of them are hydrophobic, hydrophilic, anionic, and cationic. Therefore, 4-carboxy-Tempo can find some domains to attach in highly diverse protein structure.

CHAPTER 4

CONCLUSION

In summary, force free adhesion of PEG-(N-Boc-DOPA)$_4$, their different hydrogels and BSA to SL-PS and SL-SiO_2 surfaces were studied using EPR spectroscopy.

For SL-PS surface, gradually increasing adhesion was observed with increasing concentrations of PEG-(N-Boc-DOPA)$_4$ and BSA. Hydrogel forms of PEG-(N-Boc-DOPA)$_4$ also show adhesion. Non-DOPA containing PEG showed no indication of adhesion thus, demonstrating the importance of DOPA in wet adhesion. When adhesion of hydrogels were compared, the highest adhesive performance was observed in the case of Cr_2O_7 included hydrogels with a DOPA:cross-linker concentration ratio was 1:1.

Furthermore, EPR spectra showed that hydration layers formed around hydrophilic silica nanobead surface hinder DOPA adhesion to SL-SiO_2 surface. These layers block access of PEG-(N-Boc-DOPA)$_4$ and its hydrogel derivatives to SL-SiO_2 surface except the case of $FeCl_3$ hydrogel with a DOPA:cross-linker ratio of 1:3. In addition, adhesion of BSA molecules to SL-SiO_2 was detected by EPR spectroscopy, since they contain enough hydrophobic parts to break these hydration layers.

Lastly, the line shape of free 4-carboxy-Tempo was changed only after addition of BSA and Fe^{3+} ions.

For PEG-(N-Boc-DOPA)$_4$, adhesion to PS surface is believed to be possible due to hydrophobic interaction between DOPA molecule and benzene groups. For BSA, its versatile nature due to containing different amino acid groups helped adhesion including 4-carboxy-Tempo.

In conclusion, DOPA is proved to be crucial for underwater adhesion, and EPR spectroscopy is a strong technique for investigating adhesion to different surfaces.

REFERENCES

Adams, M. Water and adhesion. International Journal of Adhesion and Adhesives 1983, 3 (2), 68–69.

Akdogan, Y.; Wei, W.; Huang, K.-Y.; Kageyama, Y.; Danner, E. W.; Miller, D. R.; Martinez Rodriguez, N. R.; Waite, J. H.; Han, S. Angewandte Chemie International Edition 2014, 53 (42), 11253–11256.

Akdogan, Y.; Emrullahoglu, M.; Tatlidil, D.; Ucuncu, M.; Cakan-Akdogan, G. EPR studies of intermolecular interactions and competitive binding of drugs in a drug–BSA binding model. Phys. Chem. Chem. Phys. 2016, 18 (32), 22531–22539.

Akdoğan, Y. Synthesis, characterization and chemical behaviour of small paramagnetic Pt species inside zeolites studied by EPR, XAS and FTIR. Ph.D. Thesis, University of Stuttgart 2009.

Anderson, T. H.; Yu, J.; Estrada, A.; Hammer, M. U.; Waite, J. H.; Israelachvili, J. N. The Contribution of DOPA to Substrate-Peptide Adhesion and Internal Cohesion of Mussel-Inspired Synthetic Peptide Films. Advanced Functional Materials 2010, 20, 4196–4205.

Barrett, D. G.; Fullenkamp, D. E.; He, L.; Holten-Andersen, N.; Lee, K. Y. C.; Messersmith, P. B. PH-Based Regulation of Hydrogel Mechanical Properties Through Mussel-Inspired Chemistry and Processing. Advanced Functional Materials 2012, 23, 1111–1119.

Bhushan, B. Biomimetics: lessons from nature-an oveview. Philosophical Transactions of the Royal Society A: Mathematical, Physical and Engineering Sciences 2009, 367, 1445-1486.

Cencer, M.; Liu, Y.; Winter, A.; Murley, M.; Meng, H.; Lee, B. P. Effect of pH on the Rate of Curing and Bioadhesive Properties of Dopamine Functionalized Poly(ethylene glycol) Hydrogels. Biomacromolecules 2014, 15 (8), 2861–2869.

Danner, E. W.; Kan, Y.; Hammer, M. U.; Israelachvili, J. N.; Waite, J. H. Adhesion of Mussel Foot Protein Mefp-5 to Mica: An Underwater Superglue. Biochemistry 2012, 51, 6511–6518.

Eberle, N; Lee, B.; Messersmith, P.B.; Westhaus, E.; Zeng, X. Synthesis and Characterization of DOPA-PEG Conjugates. Polymer Preprints. 2000 1 989-990.

Giorgioni, G.; Claudi, F.; Ruggieri, S.; Ricciutelli, M.; Palmieri, G.F.; Di Stefano, A.; Sozio, P.; Cerasa, L.S.; Chiavaroli, A.; Ferrante, C.; Orlando, G.; Glennon, R.A. Design, synthesis, and preliminary pharmacological evaluation of new imidazolinon- es as L-DOPA prodrugs. Bioorganic and Medicinal Chemistry 18 (2010) 1834–1843

Guvendiren, M.; Messersmith, P. B.; Shull, K. R. Self-Assembly and Adhesion of DOPA-Modified Methacrylic Triblock Hydrogels. Biomacromolecules 2008, 9, 122–128.

Heo, J.; Kang, T.; Jang, S. G.; Hwang, D. S.; Spruell, J. M.; Killops, K. L.; Waite, J. H.; Hawker, C. J. Improved Performance of Protected Catecholic Polysiloxanes for Bioinspired Wet Adhesion to Surface Oxides. Journal of the American Chemical Society 2012, 134, 20139–20145.

Hinderberger, D.; Jeschke, G. Site-Specific Characterization of Structure and Dynamics of Complex Materials by EPR Spin Probes. Modern Magnetic Resonance 2008, 1529– 1537.

Holten-Andersen, N.; Harrington, M. J.; Birkedal, H.; Lee, B. P.; Messersmith, P. B.; Lee, K. Y. C.; Waite, J. H. PH-Induced metal-Ligand cross-Links inspired by mussel yield self-Healing polymer networks with near-Covalent elastic moduli. Proceedings of the National Academy of Sciences 2011, 108, 2651–2655.

Hussain, T.; Rasmussen, K.; Grampp, G.; Kokorin, A. I. Effect of Viscosity on the Spin Exchange of TCNE and TEMPO Radicals with Iron(III) Acetylacetonate. Applied Magnetic Resonance 2009, 36, 121–130.

Kırpat, I.; Göksel, Y.; Karakuş, E.; Emrullahoglu, M.; Akdogan, Y. Determination of force-free wet adhesion of mussel-inspired polymer to spin labeled surface. Materials Letters 2017, 205, 48-51.

Krogsgaard, M.; Behrens, M. A.; Pedersen, J. S.; Birkedal, H. Self-Healing Mussel-Inspired Multi-pH-Responsive Hydrogels. Biomacromolecules 2013, 14 (2), 297–301.

Lee, B. P.; Dalsin, J. L.; Messersmith, P. B. Synthesis and Gelation of DOPA-Modified Poly(ethylene glycol) Hydrogels. Biomacromolecules 2002, 3 (5), 1038–1047.

Lee, B. P.; Messersmith, P.; Israelachvili, J.; Waite, J. Mussel-Inspired Adhesives and Coatings. Annual Review of Materials Research 2011, 41 (1), 99–132.

Na, H. B.; Palui, G.; Rosenberg, J. T.; Ji, X.; Grant, S. C.; Mattoussi, H. Multidentate Catechol-Based Polyethylene Glycol Oligomers Provide Enhanced Stability and Biocompatibility to Iron Oxide Nanoparticles. ACS Nano 2012, 6 (1), 389–399.

Silverman, H. G.; Roberto, F. F. Understanding Marine Mussel Adhesion. Marine Biotechnology 2007, 9 (6), 661–681.

Su, S.; Pelton, R. Bovine Serum Albumin (BSA) as an adhesive for wet cellulose. Cellulose 2006, 13, 537–545.

Stoll, S.; Schweiger, A. EasySpin, a comprehensive software package for spectral simulation and analysis in EPR. Journal of Magnetic Resonance 2006, 178, 42–55.

Talsi, E. P.; Bryliakov, K. Applications of EPR and NMR spectroscopy in homogeneous catalysis. CRC Press: Boca Raton, FL, 2017.

Tatlidil, D.; Ucuncu, M.; Akdogan, Y. Physiological concentrations of albumin favor drug binding. Phys. Chem. Chem. Phys. 2015, 17 (35), 22678–22685.

Waite, J. H. The Formation of Mussel Byssus: Anatomy of a Natural Manufacturing Process. Results and Problems in Cell Differentiation Structure, Cellular Synthesis and Assembly of Biopolymers 1992, 27–54.

Westwood, G.; Horton, N. T.; Wilker, J.J. Simplified Polymer Mimics of Cross-Linking Adhesive Proteins. Macromolecules 2007, 40, 3960–3964.

Xu, H.; Nishida, J.; Ma, W.; Wu, H.; Kobayashi, M.; Otsuka, H.; Takahara, A. Macro Letters 2012, 1, 457–460

Xu, Z. Mechanics of metal-catecholate complexes: The roles of coordination state and metal types. Scientific Reports 2013, 3 (1).

Yu, J.; Kan, Y.; Rapp, M.; Danner, E.; Wei, W.; Das, S.; Miller, D. R.; Chen, Y.; Waite, J. H.; Israelachvili, J. N. Adaptive hydrophobic and hydrophilic interactions of mussel foot proteins with organic thin films. Proceedings of the National Academy of Sciences 2013, 110, 15680–15685.

Yu, J.; Wei, W.; Menyo, M. S.; Masic, A.; Waite, J. H.; Israelachvili, J. N. Adhesion of Mussel Foot Protein-3 to TiO2 Surfaces: the Effect of pH. Biomacromolecules 2013, 14, 1072–1077.

APPENDIX A

^{1}H-NMR SPECTRA OF COMPOUNDS

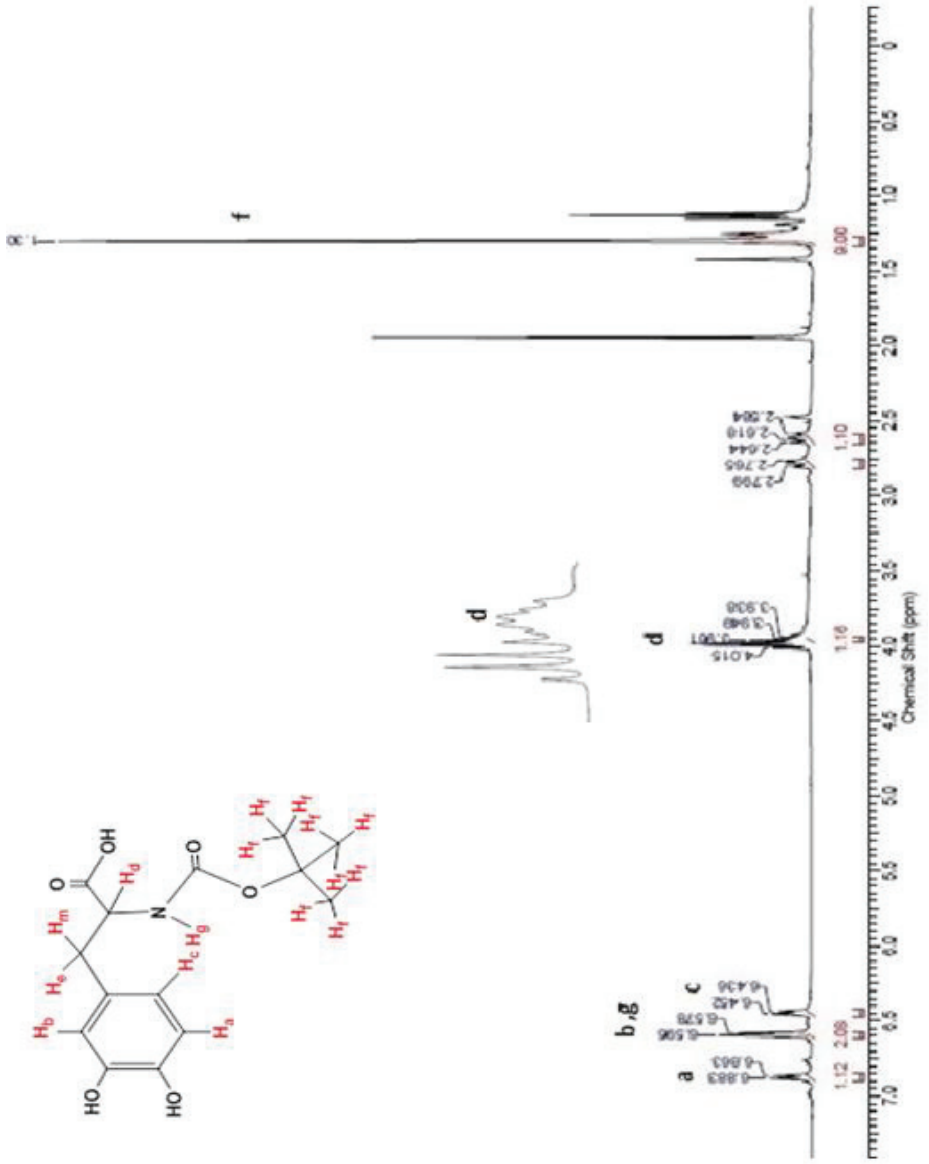

Figure A.1. ^{1}H NMR of N-Boc-DOPA molecule.

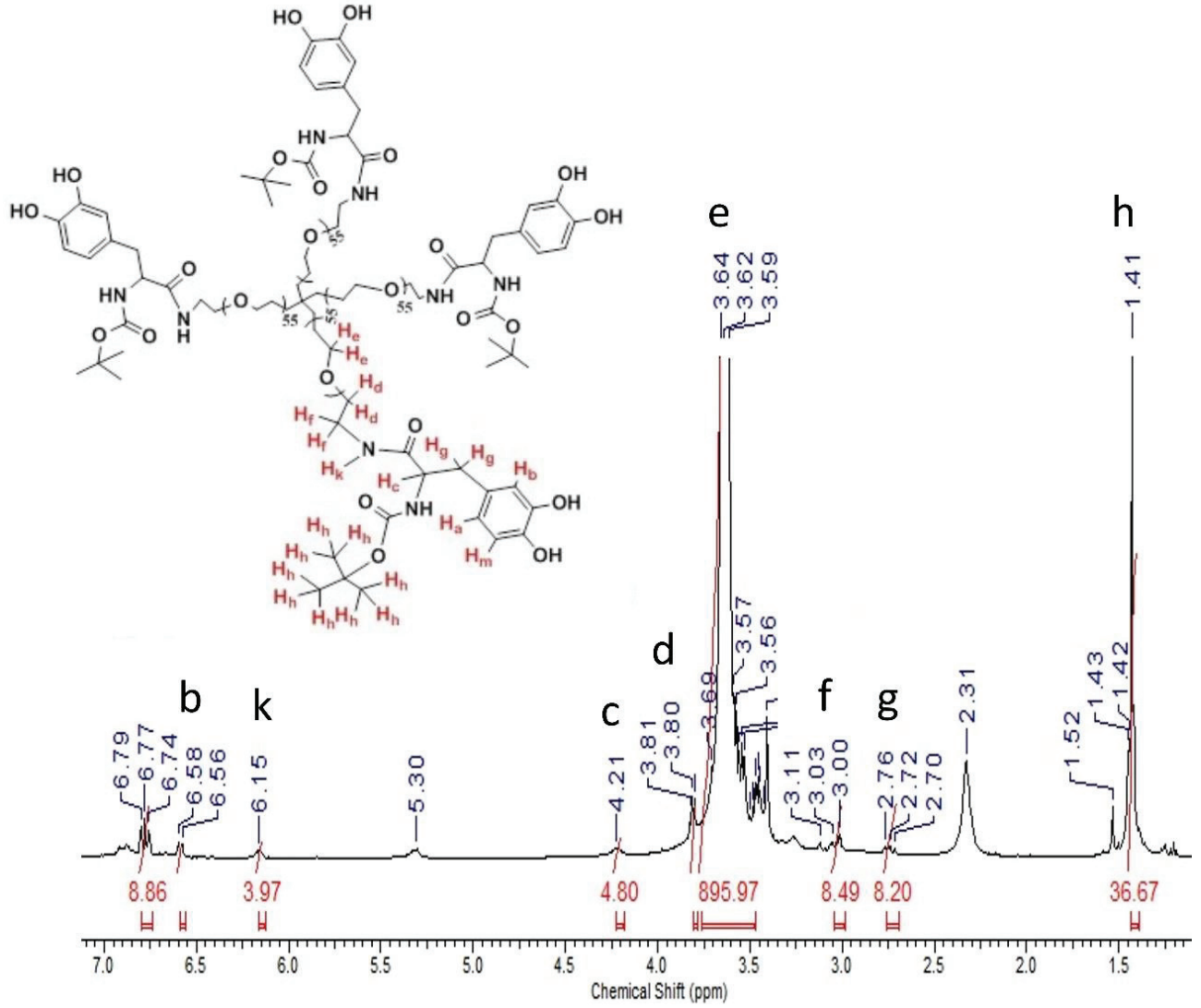

Figure A.2. ^{1}H NMR of PEG-(N-Boc-DOPA)$_4$ molecule.